AIP | The Journal of Chemical Physics

Electron attachment to POCl3. III. Measurement and kinetic modeling of branching fractions

Nicholas S. Shuman, Thomas M. Miller, A. A. Viggiano, and Jürgen Troe

Citation: The Journal of Chemical Physics **134**, 094310 (2011); doi: 10.1063/1.3549139
View online: http://dx.doi.org/10.1063/1.3549139
View Table of Contents: http://scitation.aip.org/content/aip/journal/jcp/134/9?ver=pdfcov
Published by the AIP Publishing

Electron attachment to $POCl_3$. III. Measurement and kinetic modeling of branching fractions

Nicholas S. Shuman,[1] Thomas M. Miller,[1] A. A. Viggiano,[1,a)] and Jürgen Troe[2,b)]
[1]*Air Force Research Laboratory, Space Vehicles Directorate, Hanscom Air Force Base, Bedford, Massachusetts 01731–3010, USA*
[2]*Institut für Physikalische Chemie, Universität Göttingen, Tammannstrasse 6, D-37077 Göttingen, Germany and Max-Planck-Institut für biophysikalische Chemie, Am Fassberg 11, D-37077 Göttingen, Germany*

(Received 17 November 2010; accepted 8 January 2011; published online 3 March 2011)

Electron attachment to $POCl_3$ was studied in the bath gas He over the pressure range 0.4–3.1 Torr and the temperature range 300–1210 K. Branching fractions of $POCl_3^-$, $POCl_2^-$, Cl^-, and Cl_2^- were measured. The results are analyzed by kinetic modeling, using electron attachment theory for the characterization of the nonthermal energy distribution of the excited $POCl_3^{-*}$ anions formed and chemical activation-type unimolecular rate theory for the subsequent competition between collisional stabilization of $POCl_3^{-*}$ and its dissociation to various dissociation products. Primary and secondary dissociations and/or thermal dissociations of the anions are identified. The measured branching fractions are found to be consistent with the modeling results based on molecular parameters obtained from quantum-chemical calculations. © *2011 American Institute of Physics*. [doi:10.1063/1.3549139]

I. INTRODUCTION

Electron attachment to phosphoryl chloride ($POCl_3$) is characterized by product branching fractions which depend on the temperature and the pressure of the bath gas.[1–3] This observation is taken as evidence for the intermediate formation of metastable, relatively long-lived, vibrationally highly excited $POCl_3^{-*}$ anions. The analysis of the properties of the branching fractions then may make use of the approach generally applied to unimolecular reactions with chemical activation, see e.g., Ref. 4. Essential elements of this treatment are the characterization of the primary electron attachment step, the dissociation of the excited anion, and inelastic collisional energy transfer of the excited anion. Previous investigations of the system have already followed this concept, but only rather simplified versions of modeling were employed.

In the present series of articles, we are providing a more detailed treatment than was given before. In part I,[3] new measurements of product branching fractions as functions of bath gas pressure and temperature were presented and the results were fitted by a step-ladder model for the competition between fragmentation and collisional stabilization of the intermediate excited anion $POCl_3^{-*}$. At the same time, the dependence of the attachment rate on buffer gas and electron temperature was investigated. At the simplified level of the analysis, however, the attachment process was assumed to result in thermal energy distributions of the excited intermediate before dissociation and collisional stabilization set in. Analyzing the attachment rate more carefully, such as was done in part II of our series,[5] allows one to characterize more correctly the starting distribution of the dissociation/collisional stabilization sequence. On this basis, the present part III provides an improved kinetic modeling of the system. Our measurements of the branching fractions are extended and a more detailed model for the chemical activation system is elaborated. Our treatment unavoidably is not parameter-free. However, we try to keep the number of fit parameters to a minimum and to employ expressions which have been tested previously for other systems. In this way, we provide a route to extrapolate the results beyond the range of conditions studied.

Electron attachment to $POCl_3$ is known[1–3] to lead to the anionic products $POCl_3^-$, $POCl_2^-$, $POCl^-$, Cl_2^-, and Cl^-. The mechanism forming $POCl_3^-$ and $POCl_2^-$ is assumed to be

$$e^- + POCl_3 \rightarrow POCl_3^{-*}, \tag{1.1}$$

$$POCl_3^{-*} \rightarrow POCl_2^- + Cl, \tag{1.2}$$

$$POCl_3^{-*} + M \rightarrow POCl_3^- + M. \tag{1.3}$$

Heretofore, it has not been clear whether the other products directly arise from $POCl_3^{-*}$ in its electronic ground state, from electronically excited $POCl_3^{-*}$, or from secondary dissociation of $POCl_2^-$, either through residual excitation from reaction (1.2) or thermal reactivation of $POCl_2^-$. We extend the measurements of branching fractions from part I to broader ranges of temperature in order to answer some of these questions. We also inspect the possibilities for electron autodetachment from $POCl_3^{-*}$ via

$$POCl_3^{-*} \rightarrow POCl_3 + e^-, \tag{1.4}$$

as well as the extent of thermal dissociation of $POCl_3^-$ initiated by thermal reactivation of $POCl_3^-$,

$$POCl_3^- + M \rightarrow POCl_3^{-*} + M. \tag{1.5}$$

a)Electronic mail: afrl.rvb.pa@hanscom.af.mil.
b)Author to whom correspondence should be addressed. Electronic mail: shoff@gwdg.de.

These questions require extensive kinetic modeling analogous to our previous work on the electron attachment to SF_6.[6–9] A comparison of the two reaction systems appears attractive for a number of reasons, last but not least because SF_6 has no permanent dipole moment while $POCl_3$ is markedly polar. This has consequences for the starting distribution of the dissociation/collisional stabilization sequence.

While the dissociative component of reactions (1.1)–(1.3), i.e., the dissociative attachment reaction

$$e^- + POCl_3 \rightarrow POCl_2^- + Cl \quad \Delta H = 0.00 \text{ eV}, \tag{1.6}$$

is almost thermoneutral, the products Cl^-, $Cl_2{}^-$, and $POCl^-$ are formed in endothermic processes

$$e^- + POCl_3 \rightarrow POCl_2 + Cl^- \quad \Delta H = 0.11 \text{ eV}, \tag{1.7}$$

$$e^- + POCl_3 \rightarrow POCl + Cl_2^- \quad \Delta H = 0.40 \text{ eV}, \tag{1.8}$$

and

$$e^- + POCl_3 \rightarrow POCl^- + Cl_2 \quad \Delta H = 1.53 \text{ eV}. \tag{1.9}$$

The given enthalpies of reactions (1.6)–(1.9) at 298 K are from Ref. 10 using the Gaussian G3 model chemistry and are estimated to be accurate within about ±0.1 eV, see the Appendix. In the present work, we investigate whether channels (1.7) and (1.8) like channel (1.6) proceed through vibrationally highly excited electronic ground state $POCl_3{}^{-*}$ or whether there is evidence for the participation of other pathways.

II. EXPERIMENTAL TECHNIQUE AND RESULTS

The two flowing-afterglow Langmuir-probe (FALP) apparatuses used in the present work were described in part II of this series[5] and in greater detail in earlier literature.[11–13] One apparatus was a conventional FALP apparatus normally used in the 300–550 K temperature range.[11,12] The second apparatus was a high-temperature FALP (HT-FALP, 300–1200 K). In both, we first measure the ambipolar diffusion rate, with no $POCl_3$ present, and then observe the decay of the electron density along the flow tube axis due to the coupled effects of diffusion and electron attachment to $POCl_3$, from which the electron attachment rate coefficient k_{at} is determined. Technical differences between the FALP and HT-FALP and problems related to high-temperature measurements were discussed in part II.[5] For the present work, we shall focus on matters relevant to the product branching fraction measurements. Axial apertures at the downstream ends of the flow tubes are used to pass a sample of the ion swarm into a high vacuum region for mass analysis with an rf quadrupole mass spectrometer and detection with an electron multiplier. Only relative ion intensities are needed for product branching fractions. For accurate data, account must be taken of mass discrimination effects. Possible mass discrimination sources include differential diffusion of ions in the flow tube, collisions in the lens region following the extraction aperture, differential transmission of ions by the mass spectrometer, and differential detection in the electron multiplier. In the FALP, we have determined overall mass discrimination factors using two methods that were described in Ref. 14, (a) via ion–molecule reactions, e.g., $Cl^- + SO_2 \rightarrow SO_2Cl^-$, in which the product ion intensity should equal the precursor ion intensity if no mass discrimination occurs; and (b) introducing a concentration of an electron-attaching gas (e.g., SF_6) that causes the electron density to drop by half at a fixed point beyond the reactant inlet port, and recording the resulting anion intensities for various electron-attaching gases which yield anions of different masses. With these methods, we mapped out the discrimination as a function of ion mass, and used this distribution to correct the raw ion intensities in the present $POCl_3$ experiments. Light, monatomic ions tended to be discriminated against relative to heavier polyatomic ions over the mass range of these experiments. The mass discrimination factors were found to be stable to within 10% during the course of this work as long as no significant adjustments were made to the ion lenses, mass spectrometer, or electron multiplier. Rather than repeating these experiments for the HT-FALP, we measured the branching fractions at 1.67 Torr and 500 K in both apparatuses and determined the mass discrimination factors in the HT-FALP so that the results were identical. In the HT-FALP, heavier ions are slightly discriminated against.

For rate constant measurements, the nominal buffer gas pressure in the FALP flow tube was set to *T*/300 Torr, which maintains a constant gas number density over the FALP temperature range. In order to measure the effect of buffer gas pressure on the branching fractions at 300–500 K, the FALP flow tube pump was throttled to drive the pressure as high as 8 Torr. Higher pressure appeared to begin to overload the diffusion pump on the ion lensing section of the ion sampling system. Throttling the flow tube pump caused the gas and plasma flow velocities to be proportionately reduced, so that the electron attachment reaction occurred over a shorter distance, and the ion drift time to the sampling aperture was longer. Anions do not diffuse to the flow tube walls as long as electrons are still present to handle the task, but once all electrons have attached or diffused away, anions may diffuse to the walls, possibly at different rates. Calculated and experimental ion diffusion rates in He gas roughly fit a power law ($M^{-0.51}$) dependence on ion mass M and imply that there is a difference of a factor of ∼2 in the diffusion rates for our lightest and heaviest anions (Cl^- and $POCl_3{}^-$).[15] These differences in diffusion rates (along with other discrimination factors) are taken into account empirically by the mass discrimination measurements described above, and should not change with pressure in the 1–8 Torr range. However, no mass discrimination calibrations were made specifically under the high-pressure conditions. During the pressure tests, the electric potential between the sampling aperture and the first lens element was kept low (<1 V), to minimize differential scattering in the lens region. We assign a ±10% uncertainty to the product branching fractions reported here.

Our modeling of branching fractions given below is based on three sets of experimental data: (i) branching fractions of $POCl_3{}^-$ and $POCl_2{}^-$ obtained in part I (Ref. 3) in the bath gas He in the pressure range 0.4–7 Torr and at the temperatures 297, 372, 457, and 552 K; (ii) branching

TABLE I. Measured branching fractions Y of reaction products in the electron attachment to $POCl_3$.

T/K	$Y(POCl_3^-)$	$Y(POCl_2^-)$	$Y(Cl^-)$	$Y(Cl_2^-)$
(a) [He] = 3.2×10^{16} cm^{-3}; reaction time 4.4 ms.				
300	0.25	0.74	0.012	…
400	0.10	0.89	0.02	…
500	0.035	0.93	0.03	0.002
550	0.02	0.94	0.04	0.005
(b) [He] = 1.9×10^{16} cm^{-3} (2.5×10^{16} cm^{-3} at 300 K); reaction time 2.3 ms.				
300	0.24	0.74	0.012	…
507	0.023	0.946	0.031	…
603	0.009	0.955	0.034	0.005
698	0.003	0.933	0.048	0.016
805	0.001	0.896	0.064	0.038
853	…	0.855	0.105	0.04
905	…	0.704	0.235	0.062
957	…	0.453	0.46	0.088
1031	…	0.063	0.845	0.092
1110	…	0.008	0.929	0.064
1210	…	0.002	0.94	0.056
P/Torr		(c) T = 300 K, M = He		
0.75	0.24	0.74	0.01	…
1.0	0.25	0.74	0.01	…
2.02	0.33	0.66	0.01	…
3.05	0.37	0.62	0.01	…
P/Torr		(d) T = 500 K, M = He		
0.4	0.02	0.95	0.02	0.002
0.81	0.03	0.94	0.03	0.002
1.01	0.03	0.93	0.03	0.002
2.07	0.05	0.92	0.03	0.002
3.07	0.06	0.91	0.03	0.002

fractions of $POCl_3^-$ and $POCl_2^-$ from Ref. 2 in the bath gas N_2 in the pressure range 1–760 Torr and at the temperatures 300, 373, and 423 K; (iii) branching fractions of $POCl_3^-$, $POCl_2^-$, Cl^-, and Cl_2^- from the present work in the bath gas He in the pressure range 0.4–3.1 Torr and at temperatures from 300 to 1210 K. For the data (i) and (ii), see Refs. 2 and 3. Our new results are summarized in Table I. They were taken at reaction times between 2 and 12 ms; the higher numbers refer to higher pressure. The data are discussed along with the kinetic modeling results in Section III. Confirming the results of part II,[5] we did not observe a pressure dependence of the overall rate of the attachment forming $POCl_3^-$, $POCl_2^-$, Cl^-, and Cl_2^- between 0.7 and 4 Torr. We measured this by adding small amounts of both $POCl_3$ and SF_6 and measuring the relative branching between the sum of the $POCl_3$ derived ions to SF_6^-. Since the SF_6 rate coefficient was already shown not to have a pressure dependence, this implies that neither does that for $POCl_3^-$.[6–9]

III. THEORETICAL ANALYSIS

A. Electron attachment

Attachment rate coefficients k_{at} as functions of buffer gas temperature T_{gas} and electron temperature T_{el} have been analyzed in part II (Ref. 5) in terms of electron capture theory[16–18] and "electron-phonon coupling" or "intramolecular vibrational relaxation" factors P^{IVR}. The latter were empirically fitted to the experimental data. The attachment leads to broad distributions $g(E, J)$ of the internal energy E and the total angular momentum (quantum number J) of the formed excited anions. These distributions allow one to analyze the various potential processes the anions undergo. Once the attachment rate has been analyzed such as described in part II,[5] one may quantitatively determine the $g(E, J)$. Obviously the $g(E, J)$ depend on the gas temperature T_{gas} and the electron temperature T_{el} in thermal environments. We show, however, that, even when $T_{el} = T_{gas}$, the $g(E, J)$ do not correspond to thermal distributions at the gas temperature T_{gas}. This is the issue of the present section.

The energies E_i of the vibrational states i of the neutral target and the energy E_{el} of the attaching electrons both contribute to the internal energy E of the formed anion, i.e., $E = E_i + E_{el}$. We assume that both, E_i and E_{el}, are thermally distributed. This does not mean that the energies E of $POCl_3^{-*}$ are also thermal and in the following we investigate to what extent they differ from thermal distributions at the temperature of the E_i and E_{el}.

We consider the distribution $g(E, J, T_{gas}, T_{el})$ of vibrational energies and total angular momenta of $POCl_3^{-*}$, formed by attachment of electrons (at temperature T_{el}) to $POCl_3$ (at temperature T_{gas}). As only very few partial waves of the electron contribute to the attachment,[5] J is essentially determined by the angular momentum of $POCl_3$. In the following we neglect the J-dependence and omit J. The distribution $g(E, T_{gas}, T_{el})$ is proportional to the rate coefficient $k_{at}(E, T_{gas}, T_{el})$ of attachment resulting in $POCl_3^{-*}$ at an energy E and hence to the average of the product $\sigma_{at}v$ of the attachment cross section $\sigma_{at}(E, T_{gas}, T_{el})$ and the relative velocity $v(E_{el})$ of $POCl_3$ and the electrons, i.e.,

$$g(E, T_{gas}, T_{el}) \propto \langle \sigma_{at}(E, T_{gas}, T_{el}) v(E_{el}) \rangle, \quad (3.1)$$

where E_{el} denotes the kinetic energy of the attaching electron, the energy E of $POCl_3^{-*}$ is given by $E = E_{el} + E_i$ with the vibrational energy E_i of $POCl_3$, and the averaging extends over thermal distributions of E_{el} and E_i. With $\sigma_{at}(E_{el}) \propto P(E_{el})$ and $v(E_{el}) \propto E_{el}^{1/2}$, see Ref. 6, one then has

$$g(E, T_{gas}, T_{el}) \propto \sum_{E_i=0}^{E} P(E - E_i)(E - E_i)^{-1/2} \times \exp(-E_i/kT_{gas}) \exp[-(\mathrm{E} - \mathrm{E}_i)/kT_{el}], \quad (3.2)$$

where $g(E, T_{gas}, T_{el})$ is a distribution per energy interval and $P(E_{el}) = P(E - E_i)$ is the attachment probability, including a Vogt–Wannier capture factor and an IVR factor, such as determined in Ref. 5. Comparing $g(E, T_{gas} = T_{el})$ from Eq. (3.2) with the corresponding thermal distribution [given by Eq. (3.2) with the preexponential factor $P(E - E_i)(E - E_i)^{-1/2}$ omitted], the two distributions look similar but are not identical. However, the quantum structure of the two curves makes it difficult to illustrate the differences. Replacing Eq. (3.2) by a smoothed expression with a continuous

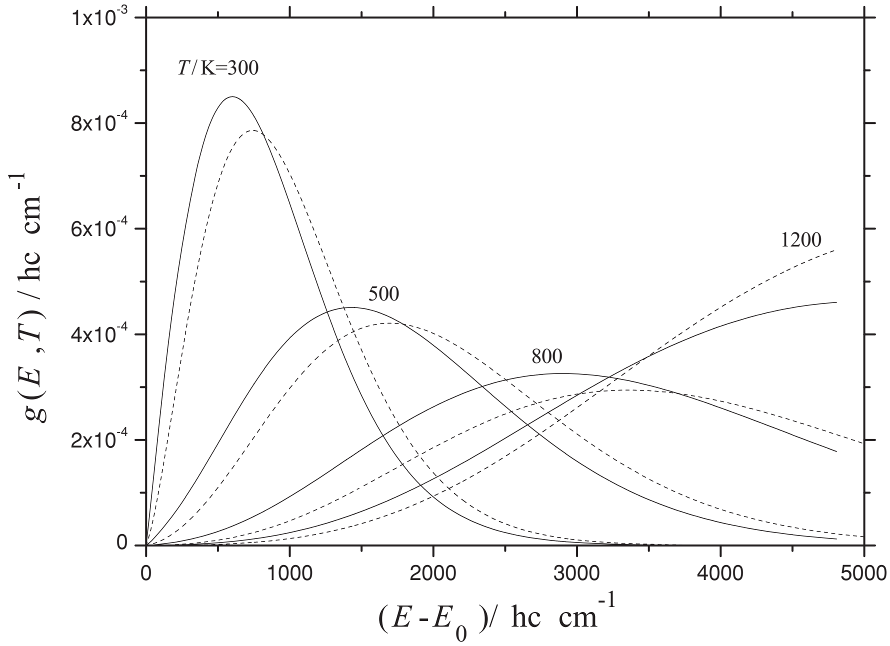

FIG. 1. Energy distributions $g(E, T)$ of $POCl_3^-$ generated by electron attachment (full lines) in comparison to thermal distributions (dashed lines) at $T = T_{el} = T_{gas}$, see text.

vibrational density of states of $POCl_3$, $\rho_{vib}(E_i)$, facilitates the representation. For this purpose, Eq. (3.2) is replaced by

$$g(E, T_{gas}, T_{el}) \propto \int_0^E P(E - E_i)(E - E_i)^{-1/2} \times \exp(-E_i/kT_{gas}) \exp[-(E - E_i)/kT_{el}] \times \rho_{vib}(E_i) dE_i. \quad (3.3)$$

The vibrational density of states $\rho_{vib}(E_i)$ is calculated in Whitten–Rabinovitch approximation,[4,19] with the vibrational frequencies of $POCl_3$ (from DFT calculations for consistency with $POCl_3^-$ frequencies, see the Appendix). Figure 1 illustrates $g(E, T_{gas} = T_{el})$ from Eq. (3.3) in comparison to the corresponding thermal distributions [from Eq. (3.3) with the preexponential factor $P(E - E_i)(E - E_i)^{-1/2}$ omitted]. By using Eq. (3.3), the differences between thermal and "kinetically generated" distributions of $POCl_3^{-*}$ are becoming more clearly visible than by using Eq. (3.2). The figure shows that the distributions generated by attachment are quasithermal; however, they correspond to slightly lower temperatures than the gas temperatures. Systematically evaluating results like those shown in Fig. 1 with respect to the positions T_{eff} of the maxima of $g(E, T)$ leads to differences between T_{eff} and $T_{gas}(=T_{el}) = $ T given approximately by

$$T_{eff} \approx 0.9\ T_{gas}. \quad (3.4)$$

One notices some narrowing of the distribution compared to a thermal distribution at T_{eff}. It should be emphasized that these results are system specific. The differences, according to Eq. (3.3), will be more pronounced for smaller and less pronounced for larger target molecules. Nevertheless, the simplification of assuming thermal distributions made in Ref. 3 in practice does not appear too serious, provided that Eq. (3.4) is obeyed. We later illustrate the quantitative consequences of reducing $T_{eff} = T_{gas}$ to $T_{eff} = 0.9\ T_{gas}$.

B. Anion dissociation (1.2) and collisional stabilization (1.3)

Having characterized the energy distribution $g(E, T)$ of $POCl_3^{-*}$ generated by the electron attachment process (1.1), we proceed to the analysis of the measured branching fractions for $POCl_3^-$ and $POCl_2^-$. We modify the analysis elaborated in part I of this series[3] in several ways. For each energy E, we express the stabilization fraction $S/(S + D)$ by

$$\left[\frac{S}{S+D}\right]_E \approx \frac{k_{stab}(E)[M]}{k_{stab}(E)[M] + k_{diss}(E)}, \quad (3.5)$$

where $k_{diss}(E)$ is the specific rate constant for the dissociation process (1.2) and $k_{stab}(E)$ denotes the effective rate coefficient for the collisional stabilization process (1.3). Like in Ref. 3, we employ a statistical adiabatic channel model/classical trajectory (SACM/CT) approach[20–25] for the characterization of $k_{diss}(E)$. We express $k_{diss}(E)$ by

$$k_{diss}(E) = f_{rigid}^{tot}(E)\, k(E)^{PST}, \quad (3.6)$$

where $k(E)^{PST}$ is obtained from phase space theory (PST) and the total rigidity factor $f_{rigid}^{tot}(E)$, being smaller than unity, accounts for the anisotropy of the potential. The determination of $k(E)^{PST}$ follows the method outlined in Ref. 26 and is not repeated here. However, compared to part I (Ref. 3) we employ a different method for the representation of the rigidity factor $f_{rigid}^{tot}(E)$. The functional form of $f_{rigid}^{tot}(E)$ is not obvious. Since publishing part I, in an analysis of halobenzene cation dissociations[24] we have gained more experience with simplified one-fit parameter expressions to determine

$f^{tot}_{rigid}(E)$ via a partial rigidity factor $f^{trans}_{rigid}(E)$ of only the transitional modes. Following this work, in contrast to part I we now express $f^{trans}_{rigid}(E)$ in the form

$$f^{trans}_{rigid}(E) = (1 - f_\infty)\exp[-(E - E_0)/c_{loose}] + f_\infty, \quad (3.7)$$

i.e., in a procedure which we term[24] SSACM (simplified SACM). As the present dissociation also produces a neutral atom and an ion like in halobenzene cation dissociations, we expect a similarly good performance of Eq. (3.7) as in Ref. 24. Once the parameter c_{loose} is fitted at one energy, it is applicable for all other conditions. E_0 is the dissociation energy at 0 K. The high-energy limiting value f_∞ is estimated as $f_\infty = B_\infty(E - E_0 + E_z^*)/(s - 1)h\nu_1 h\nu_2$ where B_∞ is the geometrical mean of the rotational constants (in energy units) of $POCl_2^-$, $h\nu_1$ and $h\nu_2$ are the two transitional mode quanta of $POCl_3^-$ turning into free rotations of $POCl_2^-$ (see the Appendix), s is the number of oscillators of $POCl_3^-$, and E_z^* is the zero-point energy of rigid activated complex $POCl_3^-$ dissociating to $POCl_2^- + Cl$. This expression for f_∞, for the case of an atom loss, mimics the transition from PST to rigid activated complex RRKM (Rice—Ramsperger–Kassel–Marcus) theory when the parameter c_{loose} approaches zero. (For the case of the loss of a diatomic fragment, the analogous expression is constructed following Ref. 26).

Employing the molecular parameters of $POCl_3^-$ and $POCl_2^-$ given in the Appendix, $k_{diss}(E)$ is calculated for a variety of values of the fit parameter c_{loose} and the results are shown in Fig. 2. $k(E)^{PST}$ from phase space theory, which corresponds to $c_{loose} \rightarrow \infty$, determines the upper limit for $k_{diss}(E)$. The special form of $f^{trans}_{rigid}(E)$, such as given by Eq. (3.7) and termed SSACM, is responsible for the observation that $k_{diss}(E)$ approaches $k(E)^{PST}$ near $E = E_0$ and with increasing energy decreases toward values corresponding to RRKM theory.

The competition between dissociation (1.2) and collisional deactivation proceeds as a multistep process and can be described by a master equation. However, the finer details of the collisional deactivation and the dissociation are not known. Therefore, we simplify the approach by replacing the master equation by a step-ladder model as we did previously in part I.[3] It was shown in Ref. 27 that the two approaches are nearly equivalent when the step size is chosen as the average total energy $\langle\Delta E\rangle$ transferred per collision (up- and down-transitions included). For a starting energy E, then the branching fraction $Y = S/(S + D)$ for stabilization S (competing with dissociation D) is given by

$$Y(E) = \left(\frac{S}{S + D}\right)_E = \prod_{i=1}^{T(E)} \frac{Z[M]}{Z[M] + k(E - (i - 1)|\langle\Delta E\rangle|)}, \quad (3.8)$$

where $T(E) = \text{Integer}[(E - E_0)/|\langle\Delta E\rangle|] + 1$ denotes the number of steps between E and energies below E_0 required for stabilization. $Y(E)$ finally has to be averaged over the starting energy distribution derived in Sec. III A. Z is the appropriate total collision frequency for energy transfer, here being given by the Langevin collision frequency between $POCl_3^{-*}$ and the bath gas M (see the Appendix). It was shown that,

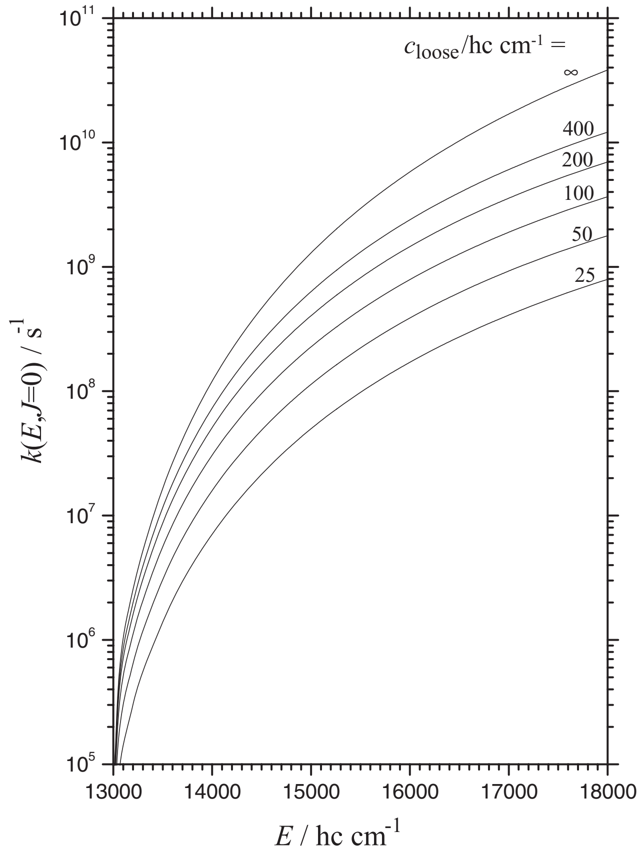

FIG. 2. Specific rate constants $k(E, J = 0)$ for the dissociation of $POCl_3^{-*} \rightarrow POCl_2^- + Cl$. Modeling by simplified statistical adiabatic channel model [SSACM, see Eq. (3.7)] with various rigidity fit parameters c_{loose} [$c_{loose} \rightarrow \infty$ corresponds to phase space theory (PST)].

in the high pressure limit with substantial collisional stabilization, Eq. (3.8) approaches a linear Stern–Volmer-type dependence of $1/Y(E)$ on [M] while a nonlinear dependence is typical for small stabilization yields at very low pressures. Averaging $Y(E)$ over broad starting distributions $g(E)$ of energies like illustrated in Sec. III A results in more pronounced nonlinearities over the complete pressure range. In Sec. III C we represent our modeling results of the averaged stabilization fraction

$$\langle Y\rangle = \int_0^\infty g(E, T)\, Y(E)\, dE, \quad (3.9)$$

by plotting $\langle Y\rangle^{-1}$ as a function of [M] in a Stern–Volmer-type representation. Besides the parameter c_{loose} of $k(E)$, we then have a second parameter $\langle\Delta E\rangle$. We keep the two parameters constant for all conditions and test whether the experimental results are reproduced over wide ranges of conditions without further parameter changes. It turns out that the parameters cannot be fitted independently. Instead, different pairs of parameters fit the experiments equally well, see below.

C. Modeled stabilization fractions

Combining the present experimental stabilization fractions $\langle S/(S+D)\rangle$ with those of Refs. 2 (for M = N_2) and 3 (for M = He), we first fit measurements of pressure de-

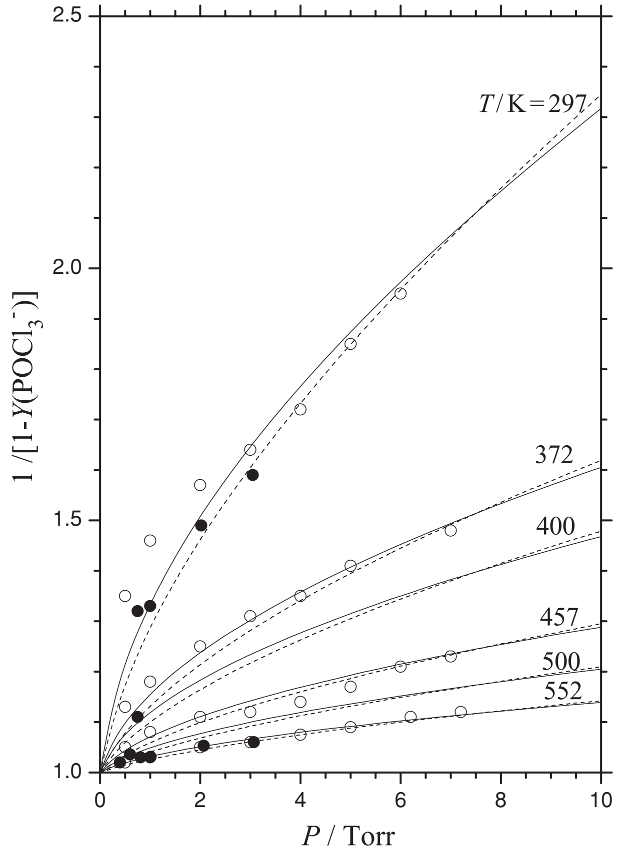

FIG. 3. Measured and modeled branching parameters $1/[1 - Y(POCl_3^-)]$ in the electron attachment to $POCl_3$ in the bath gas He [full circles: present work, open circles: Ref. 3, dashed lines: phase space theory (PST) with energy transfer step size $-\langle \Delta E \rangle$/hc = 150 cm^{-1}, full lines: rigidity fit parameter c_{loose}/hc = 25 cm^{-1} and $-\langle \Delta E \rangle$/hc = 10 cm^{-1}; see text].

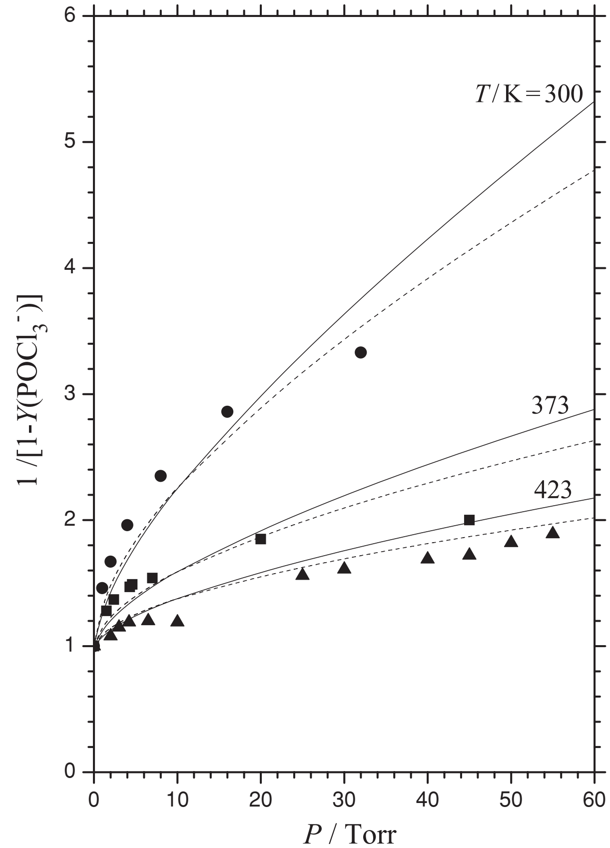

FIG. 4. As Fig. 3, but for the bath gas N_2 [experimental points from Ref. 2, dashed lines: PST with $-\langle \Delta E \rangle$/hc = 120 cm^{-1}, full lines: (c_{loose}/hc, $-\langle \Delta E \rangle$/hc) = (25 cm^{-1}, 8 cm^{-1})].

pendences of branching fractions at fixed temperatures under conditions where Cl^- and Cl_2^- formations are almost negligible. This first part of the analysis covers the temperature range 300–550 K. Higher temperatures are considered later in Sec. III D.

We employ the Stern–Volmer-type representation $1/[1-Y(POCl_3^-)]$ as a function of the pressure P where $Y(POCl_3^-)$ corresponds to $\langle S/(S+D) \rangle$, see Eqs. (3.8) and (3.9). Figure 3 compares the combined experimental results of the present work and of part I,[3] for the bath gas He, with the present modeling. One indeed notices the marked curvature of the plots which is the consequence of the broad energy distribution of $POCl_3^{-*}$ generated by the attachment process. Additional small curvatures for $Y(POCl_2^-) \rightarrow 1$ occur at very low pressures. Those are due to the multistep character of the process which can be neglected over our range of conditions.[27] There are only small differences between our present results (full circles in Fig. 3) and our previous measurements[3] (open circles in Fig. 3). As mentioned above, one notices that different pairs of fit parameters (c_{loose}, $\langle \Delta E \rangle$) fit the Stern–Volmer-type plots equally well. Figure 3 compares ($c_{loose} \rightarrow \infty$, $-\langle \Delta E \rangle$/hc = 150 cm^{-1}), corresponding to phase space theory in $k(E)$ (dashed lines), with (c_{loose}/hc = 25 cm^{-1}, $-\langle \Delta E \rangle$/hc = 10 cm^{-1}) (full lines). The modeling with (c_{loose}/hc = 100 cm^{-1}, $-\langle \Delta E \rangle$/hc = 42 cm^{-1}) is between these cases and is not shown. The order of magnitude of $-\langle \Delta E \rangle$/hc, with its maximum of 150 cm^{-1} for PST in $k(E)$, is consistent with the conclusion that collisional energy transfer of excited ions is far from being "strong." It is rather of similar character to the "weak" collisional energy transfer observed for excited neutral molecules.[28–32]

The results of Ref. 2 with the bath gas N_2, extending over the temperature range 300–423 K and employing pressures up to 1 bar, have been evaluated previously in part I.[3] We reevaluated them in the present work using our improved modeling scheme. As the $1/Y(POCl_2^-)$ versus pressure plot exaggerates experimental scatter at high pressures, we limited our Stern–Volmer-type representation of the data to pressures below 60 Torr. Figure 4 illustrates our new modeling results for two pairs of the parameters (c_{loose}, $\langle \Delta E \rangle$). Slightly surprisingly we find that essentially the same parameter pairs with the same $\langle \Delta E \rangle$ represent the results within the experimental scatter. For example, Fig. 4 shows results for (c_{loose}/hc, $-\langle \Delta E \rangle$/hc) = ($\infty$, 120 cm^{-1}; dashed lines) and (25 cm^{-1}, 8 cm^{-1}; full lines). Similar values of $\langle \Delta E \rangle$ in M = He and N_2 in some cases have also been observed with excited neutral molecules, see e.g., Ref. 28, although He in most cases was found to be less efficient than N_2 (see e.g., Refs. 29 and 30 and references cited therein). The temperature dependences of Figs. 3 and 4 also illustrate the consequences of reducing $T_{eff} = T_{gas}$ to $T_{eff} = 0.9\ T_{gas}$ such as given by Eq. (3.4). A reduction of T_{eff} by

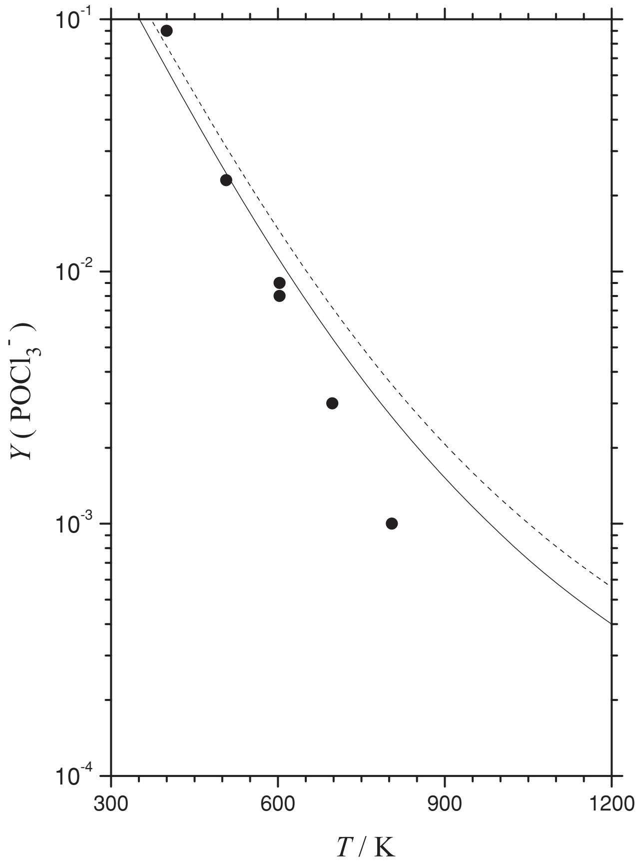

FIG. 5. As Fig. 3, with experiments and modeling from the present work for [He] = 1.9×10^{16} cm^{-3} [dashed line: PST with $-\langle\Delta E\rangle$/hc = 150 cm^{-1}, full line: (c_{loose}/hc, $-\langle\Delta E\rangle$/hc) = (25 cm^{-1}, 10 cm^{-1})].

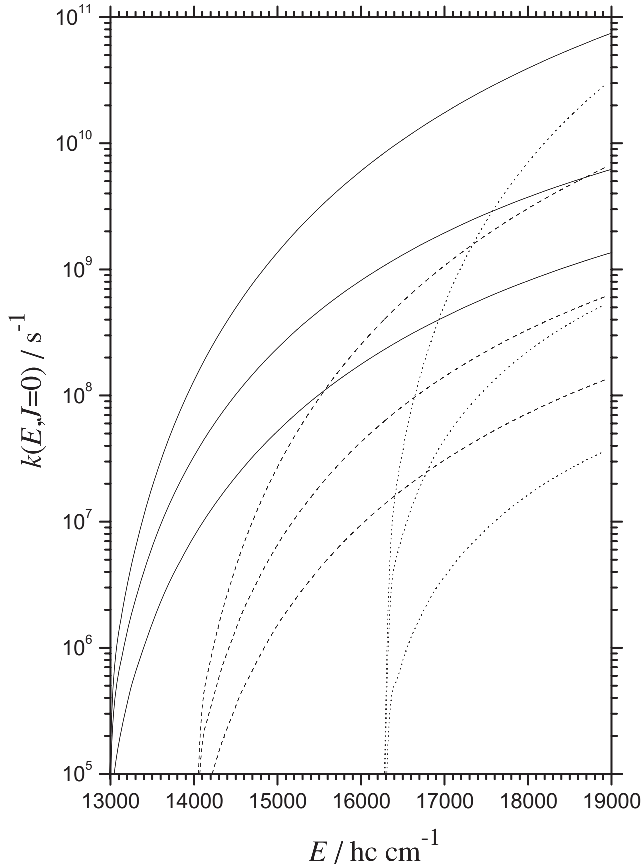

FIG. 6. SSACM modeling of specific rate constants $k(E, J = 0)$ for dissociations of $POCl_3^-$ [full lines: $POCl_3^- \rightarrow POCl_2^- + Cl$, Eq. (1.6); dashed lines: $POCl_3^- \rightarrow POCl_2 + Cl^-$, Eq. (1.7), dotted lines: $POCl_3^- \rightarrow POCl + Cl_2^-$, Eq. (1.8); within each group of three lines, the rigidity fit parameter in Eq. (3.7) is varied from c_{loose}/hc = ∞ (top, PST), 100 cm^{-1} (middle), to 25 cm^{-1} (bottom); see text].

10%, e.g., in Fig. 3 would be quite visible. It would have to be compensated by increasing the fitted $\langle\Delta E\rangle$ by about 50% when agreement with the experiments is intended.

D. High temperature results

At temperatures above about 600 K, additional pathways become important and influence the measured branching fractions. We first analyze the yield of $POCl_3^-$, before we proceed to the reaction products $POCl_2^-$, Cl^-, and Cl_2^-.

Figure 3 illustrates very good agreement between measured and modeled yields of $POCl_3^-$ and $POCl_2^-$ over the range 297–552 K. An extension of the modeling to the range 600–1200 K studied in the present work shows increasing differences between measured and modeled branching fractions of $POCl_3^-$. Above 800 K, no $POCl_3^-$ is observed above the experimental threshold of $Y(POCl_3^-) = 10^{-3}$. Figure 5 illustrates this observation. With decreasing stabilization yields the step-ladder model in principle may become inaccurate. However, from what follows later a different explanation appears more probable. At temperatures above about 600 K, collisionally stabilized $POCl_3^-$ may be reactivated in collisions with the buffer, see Eq. (1.5) which leads to thermal dissociation under the conditions of the present experiments. As there are only few results, we have not modeled the falloff curve for this reaction. However, a crude estimate of a high pressure thermal dissociation rate constant of 10^{16} exp(-1.6 eV/RT) s^{-1} indicates that thermal dissociation should be fast at temperatures above 600 K. There is the second possibility that the effective $k(E)$ in the step-ladder equation (3.8), at the higher energies reached at higher temperatures, increases because of the onset of reactions (1.7) and (1.8). In order to analyze this possibility more quantitatively, specific rate constants $k(E)$ for the formation of Cl^- and Cl_2^- are modeled in the following.

Using the molecular parameters given in the Appendix, SSACM calculations of $k(E)$ for the reactions of Eqs. (1.6)–(1.8) have been made and illustrated in Fig. 6. Again there is the uncertainty of the SSACM rigidity fit parameter c_{loose}. However, a comparison of the PST curves ($c_{loose} \rightarrow \infty$) of the three channels provides already some hints. Only if c_{loose} for reaction (1.6) would be very much smaller than c_{loose} for the reactions (1.7) and (1.8), then this could explain the points in Fig. 5 at T larger than 600 K. However, this is ruled out below.

With the modeled $k(E)$ for reactions (1.7) and (1.8) one may now analyze the branching fractions for Cl^- and Cl_2^- formation. A first step in this direction is the comparison of measured branching fractions (obtained essentially in the absence of collisional stabilization of $POCl_3^-$) with modeling results for $Y_i = k_i(E)/\sum k_i(E)$ using $k_i(E)$ obtained by phase

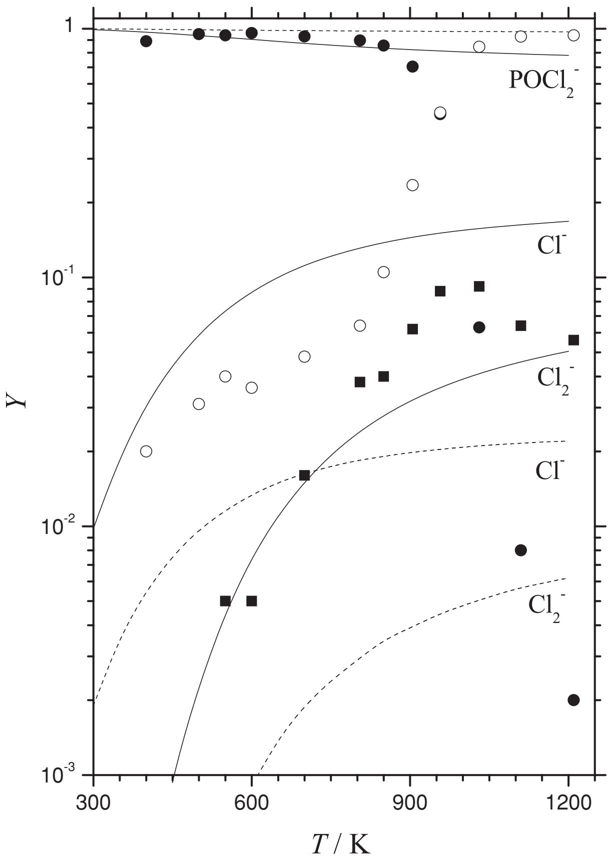

FIG. 7. Branching fractions Y of $POCl_2^-$, Cl^-, and Cl_2^- from electron attachment to $POCl_3^-$ at low bath gas pressures [essentially no collisional stabilization; experimental points from this work for $POCl_2^-$ (●), Cl^- (◯), and Cl_2^- (■); modeling results with $k(E, J = 0)$ from phase space theory (dashed lines); modeling results with c_{loose}/hc = 100 cm^{-1} for $POCl_2^-$ formation and PST for Cl^- and Cl_2^- formation (full lines); see text].

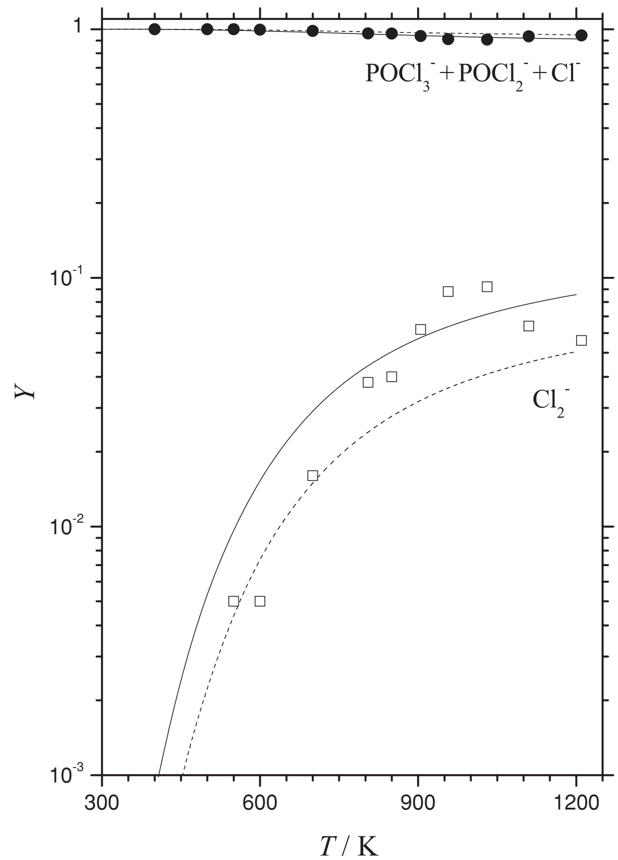

FIG. 8. Branching fractions Y for ($POCl_3$ + $POCl_2^-$ + Cl^-) and Cl_2^-, as Fig. 7 [full lines for E_0 ($POCl_3^- \rightarrow POCl + Cl_2^-$) = 1.98 eV, dashed lines for E_0 ($POCl_3^- \rightarrow POCl + Cl_2^-$) = 2.01 eV].

space theory, see the dashed lines in Fig. 7. The most striking difference is the marked decrease of $Y(POCl_2^-)$ and increase of $Y(Cl^-)$ at temperatures above about 700 K. This observation cannot be attributed to failures of the $k(E)$ calculations. Instead a secondary fragmentation of $POCl_2^-$ must take place via

$$POCl_2^- \rightarrow POCl + Cl^-, \tag{3.10}$$

which destroys $POCl_2^-$ nearly completely at 1200 K. There are two possibilities for this fragmentation, either thermal dissociation analogous to the thermal dissociation of $POCl_3^-$ such as illustrated in Fig. 5 or dissociation by secondary chemical activation, using residual vibrational excitation from the energy partitioning between the products of the primary dissociation of $POCl_3^-$. As the dissociation energy of $POCl_2^-$ (1.70 eV) is only slightly higher than that of $POCl_3^-$ (1.60 eV), thermal dissociation is the more probable pathway. The next step is to modify the $k_i(E)$ from the PST values. When c_{loose}/hc for $POCl_2^-$ formation is lowered to 100 cm^{-1} and $k_i(E)$ for Cl^- and Cl_2^- formation are left unchanged at PST values, the full lines in Fig. 7 are obtained. Apart from the high temperature effects associated with $POCl_2^-$ dissociation, the agreement with Cl^- and Cl_2^- yields now is much better [one may attribute again the decrease of $Y(Cl_2^-)$ at temperatures above 1000 K to thermal dissociation: the dissociation energy of Cl_2^-, 1.29 eV, is smaller than that of $POCl_3^-$ or $POCl_2^-$, but the dissociation here would be in the low pressure limiting range such that higher temperatures are required for dissociation]. For a fine-tuning, in Fig. 8 we compare the combined branching fraction [$Y(POCl_3^-)$ + $Y(POCl_2^-)$ + $Y(Cl^-)$], accounting for reactions (1.6), (1.7), and (3.10), and $Y(Cl_2^-)$ with modeling results. For reaction (1.6) we employ c_{loose}/hc = 100 cm^{-1}, while for reactions (1.7) and (1.8) we use PST (values). The modeling sensitively depends on the dissociation energies of $POCl_3^-$. If the G3 value of 2.01 eV for Cl_2^- formation by reaction (1.8) (dashed lines in Fig. 8) is lowered to 1.98 eV, the full lines in Fig. 8 are obtained. In view of the 0.1 eV uncertainty of the G3 calculations, the agreement with the experiments appears quite acceptable.

One may ask why PST modeling for the reactions $POCl_3^- \rightarrow POCl_2 + Cl^-$ and $POCl_3^- \rightarrow POCl + Cl_2^-$ is acceptable while SSACM with considerable rigidity (c_{loose}/hc = 100 cm^{-1}) is employed for $POCl_3^- \rightarrow POCl_2^- + Cl$. The difference can be attributed to the polarizability of the neutral fragments, which for Cl ($\alpha = 2.18 \times 10^{-24}$ cm^3) is markedly smaller than for POCl ($\alpha = 6.10 \times 10^{-24}$ cm^3) and $POCl_2$ ($\alpha = 8.5 \times 10^{-24}$ cm^3) such that stronger isotropic long-range potentials in reactions (1.7) and (1.8) may produce a smaller anisotropy of the overall potential which results in larger values of the rigidity fit parameter c_{loose} to be used in the SSACM calculations.

IV. CONCLUSIONS

The present work illustrates the necessity to perform a detailed kinetic modeling of the electron attachment processes when metastable anions are formed as intermediates. Even when the anions are not stabilized by collisions (or radiation), the fragments may undergo secondary dissociations employing residual energy from the primary dissociation. In the presence of collisions, thermal dissociations may also take place and gain importance with increasing temperature. The present analysis of electron attachment to $POCl_3$ has illustrated the variety of possible pathways and its modeling by unimolecular rate theory. This modeling is not parameter-free. However, the present approach has limited the number of fit parameters to a minimum. Once the parameters are fixed, extrapolations of experimental data over wide ranges of conditions can be made.

Analyzing the dynamics of the metastable anions generated in electron attachment by chemical activation-type unimolecular rate theory requires knowledge of their energy distributions. The present work has demonstrated that this distribution is nearly thermal, but that its effective temperature is lower than the electron and gas temperature. In order to determine the distribution, the electron attachment rate coefficients have to be known over a wide range and have to be analyzed. In part II of this series, this was done in the framework of electron capture theory leading to empirical electron–phonon coupling factors (IVR factors) which then are used for the determination of the energy distribution of the excited anions formed by attachment.

The present series of three articles (Refs. 3, 5, and the present work) on electron attachment to the polar target $POCl_3$ nicely complements our earlier series (Refs. 6–8) on electron attachment to the nonpolar target SF_6. The polarity influences the attachment rate but the kinetic modeling of the processes of the anions formed is largely independent of this quantity. We showed that the complexity of the two attachment systems can be unraveled when the kinetic modeling is done on a very detailed level. In this way, the two systems present useful prototypes for the analysis of electron attachment dynamics with intermediate stabilizable anion formation.

ACKNOWLEDGMENTS

Helpful discussions of this work with H. Hotop and technical help of this work by A. Maergoiz is gratefully acknowledged. The project was funded by the United States Air Force of Scientific Research under Project 2303EP. Financial support by the European Office of Aerospace Research and Development (Grant Award No. FA8655-10-1–3057) is also gratefully acknowledged. T.M.M. is under contract (No. FA8718-10-C-0002) from the Institute for Scientific Research of Boston College.

APPENDIX: MOLECULAR PARAMETERS USED IN MODELING

Frequencies (in cm^{-1}). $POCl_3$: 1304.4, 561.1 (2), 456.4, 322.1 (2), 256.0, 181.1 (2); $POCl_3^-$: 1232.1, 401.1, 383.2, 268.7, 208.2, 172.9, 133.7, 80.8, 39.6; $POCl_2$: 1216.4, 509.7, 454.0, 312.8, 264.9, 182.7; $POCl_2^-$: 1201.3, 392.3, 329.6, 250.8, 199.0, 127.2; POCl: 1273.3, 477.4, 296.7; Cl_2^-: 201.0 [all from B3LYP/6–311+G (3df) calculations with scaling factor 0.989].

Rotational constants (in cm^{-1}). $POCl_2^-$: 0.1481, 0.0776, 0.0550; $POCl_2$: 0.1708, 0.0890, 0.0610; POCl: 1.108, 0.1477, 0.1303; Cl_2^-: 0.1316 ($\sigma = 2$).

Dissociation energies (at 0 K, in eV). Cl-$POCl_2^-$: 1.60; $POCl_2$-Cl^-: 1.73; POCl-Cl_2^-: 2.01; POCl-Cl^-: 1.70; $Cl_2^- \rightarrow Cl^- + Cl$: 1.29, from GAUSSIAN 03 calculations, see also Ref. 10.

PST calculations with $W(E, J = 0) \approx E/B_1$ for transitional modes leading to an atom and a spherical top (B_1) and $W(E, J = 0) \approx (E^2/2B_1^{3/2}B_2^{1/2})$ arc $\sin[B_1/(B_1 + B_2)]^{1/2}$ for transitional modes leading to a linear molecule (B_2) and a spherical top (B_1); B_1 = geometrical mean of rotational constants: $B_1(POCl_2^-) = 0.0858$, $B_1(POCl_2) = 0.0975$, $B_1(POCl) = 0.277$ cm^{-1}; see Ref. 26. Frequencies of transitional modes becoming free rotors: 80.8 and 133.7 cm^{-1} for $POCl_3^- \rightarrow POCl_2^- + Cl$.

Langevin rate constants for $POCl_3^{-*} + M$: 5.37×10^{-10} cm^3 s^{-1} (M = He) and 6.37×10^{-10} cm^3 s^{-1} ($M = N_2$).

Polarizabilities (in 10^{-24} cm^3). $POCl_2$: 8.51, POCl: 6.10, from B3LYP/6–311 +G(3df) calculations; Cl: 2.18 from Ref. 33. Dipole moment of $POCl_3$: 2.54($\pm$0.5)D from Ref. 34.

[1] T. M. Miller, J. V. Seeley, W. B. Knighton, R. F. Meads, A. A. Viggiano, R. A. Morris, J. M. Van Doren, J. Gu, and H. F. Schaefer, J. Chem. Phys. **109**, 578 (1998).
[2] D. H. Williamson, C. A. Mayhew, W. B. Knighton, and E. P. Grimsrud, J. Chem. Phys. **113**, 11035 (2000).
[3] J. M. van Doren, J. F. Friedman, T. M. Miller, A. A. Viggiano, S. Denifl, P. Scheier, T. D. Märk, and J. Troe, J. Chem. Phys. **124**, 124322 (2006) (part I of this series).
[4] T. Baer and W. L. Hase *Unimolecular Reaction Dynamics. Theory and Experiments* (Oxford University Press, Oxford, New York, 1996).
[5] N. S. Shuman, T. M. Miller, A. A. Viggiano, and J. Troe, "Electron attachment to $POCl_3$. II. Dependence of the attachment rate coefficients on gas and electron temperature," Int. J. Mass Spectrom. (in press).
[6] J. Troe, T. M. Miller, and A. A. Viggiano, J. Chem. Phys. **127**, 244303 (2007).
[7] J. Troe, T. M. Miller, and A. A. Viggiano, J. Chem. Phys. **127**, 244304 (2007).
[8] A. A. Viggiano, T. M. Miller, J. F. Friedman, and J. Troe, J. Chem. Phys. **127**, 244305 (2007).
[9] T. M. Miller, A. A. Viggiano, and J. Troe, J. Phys.: Conf. Ser. **115**, 012019 (2008).
[10] W. B. Knighton, T. M. Miller, E. P. Grimsrud, and A. A. Viggiano, J. Chem. Phys. **120**, 211 (2004).
[11] J. F. Friedman, T. M. Miller, J. K. Friedman-Schaffer, A. A. Viggiano, G. K. Rekha, and A. E. Stevens, J. Chem. Phys. **128**, 104303 (2008).
[12] T. M. Miller, Adv. At., Mol., Opt. Phys. **51**, 299 (2005).
[13] T. M. Miller, J. F. Friedman, J. S. Williamson, L. C. Schaffer, and A. A. Viggiano, Rev. Sci. Instrum. **80**, 034104 (2009).
[14] N. S. Shuman, T. M. Miller, C. M. Caples, and A. A. Viggiano, J. Phys. Chem. A **114**, 11100 (2010).
[15] K. Dryahina and P. Španěl, Int. J. Mass Spectrom. Ion Process. **244**, 148 (2005).
[16] E. I. Dashevskaya, I. Litvin, E. E. Nikitin, and J. Troe, Phys. Chem. Chem. Phys. **10**, 1270 (2008).
[17] E. E. Nikitin and J. Troe, Phys. Chem. Chem. Phys. **12**, 9011 (2010).
[18] E. I. Dashevskaya, I. Litvin, E. E. Nikitin, and J. Troe, "Electron capture by polarizable dipolar targets: Numerical and analytically approximated capture probabilities," J. Phys. Chem. A (in press).

[19]W. Forst, *Theory of Unimolecular Reactions* (Academic, New York, 1973).
[20]A. I. Maergoiz, E. E. Nikitin, J. Troe, and V. G. Ushakov, J. Chem. Phys. **117**, 4201 (2002).
[21]J. Troe, V. G. Ushakov, and A. A. Viggiano, Z. Phys. Chem. **219**, 699 (2005).
[22]J. Troe, V. G. Ushakov, and A. A. Viggiano, Z. Phys. Chem. **219**, 715 (2005).
[23]J. Troe, V. G. Ushakov, and A. A. Viggiano, J. Phys. Chem. A **110**, 1491 (2006).
[24]W. Stevens, B. Sztáray, N. Shuman, T. Baer, and J. Troe, J. Phys. Chem. A **113**, 573 (2009).
[25]J. Troe, Z. Phys. Chem. **223**, 347 (2009).
[26]J. Troe, J. Chem. Phys. **79**, 6017 (1983).
[27]J. Troe, J. Phys. Chem. **87**, 1800 (1983).
[28]M. Heymann, H. Hippler, H. J. Plach, and J. Troe, J. Chem. Phys. **87**, 3867 (1987).
[29]U. Hold, T. Lenzer, K. Luther, and A. C. Symonds, J. Chem. Phys. **119**, 11192 (2003).
[30]T. Lenzer, K. Luther, D. Nilsson, and S. Nordholm, J. Phys. Chem. B **109**, 8325 (2005).
[31]L. A. Miller and J. R. Barker, J. Chem. Phys. **105**, 1383 (1996).
[32]L. A. Miller, C. D. Cook, and J. R. Barker, J. Chem. Phys. **105**, 3012 (1996).
[33]T. M. Miller and B. Bederson, Adv. At. Mol. Phys. **13**, 1 (1977).
[34]*Handbook of Chemistry and Physics*, 85th ed., edited by D. R. Lide (CRC Press, Boca Raton, 2004).